doi: 10.4149/gpb_2024007

Trivalent anions as probes of the CFTR channel pore

Paul Linsdell[1]

[1] *Department of Physiology and Biophysics, Dalhousie University, Halifax, Nova Scotia, Canada*

Abstract. The cystic fibrosis transmembrane conductance regulator (CFTR) Cl^- channel uses positively charged amino-acid side-chains to form binding sites for permeating anions. These binding sites have been investigated experimentally using a number of anionic probes. Mutations that alter the distribution of positive and negative charges within the pore have differential effects on the binding of monovalent *versus* divalent anions. This study uses patch clamp recording from wild-type and pore-mutant forms of CFTR to investigate small trivalent anions ($Co(NO_2)_6^{3-}$, $Co(CN)_6^{3-}$ and $IrCl_6^{3-}$) as potential probes of anion binding sites. These anions caused weak block of Cl^- permeation in wild-type CFTR (Kd ≥ 700 μM) when applied to the intracellular side of the membrane. Mutations that increase the density of positive charge within the pore (E92Q, I344K, S1141K) increased the binding affinity of these anions 80–280-fold, and also greatly increased the voltage-dependence of block, consistent with fixed charges in the pore affecting monovalent : multivalent anion selectivity. However, high-affinity pore block by $Co(NO_2)_6^{3-}$ apparently did not alter channel gating, a hallmark of high-affinity binding of divalent $Pt(NO_2)_4^{2-}$ ions within the pore. This work increases the arsenal of probes available to investigate anion binding sites within Cl^- channel pores.

Key words: Anion selectivity — Channel block — Chloride channel — Cystic fibrosis transmembrane conductance regulator — Ion binding

Introduction

Cystic fibrosis (CF) is caused by loss-of-function mutations in the CF transmembrane conductance regulator (CFTR), an epithelial cell anion channel (Ong and Ramsey 2023). The mechanism of Cl^- permeation in CFTR has been studied in detail by a combination of structural, functional, and computational methods (Linsdell 2017; Hofmann et al. 2018; Hwang et al. 2018; Zhang et al. 2018; Csanády et al. 2019; Farkas et al. 2020; Zeng et al. 2023). Permeating Cl^- ions enter the pore from the cytoplasm *via* a single lateral portal, then pass through a wide inner vestibule before the pore narrows to form a restricted region or "selectivity filter" close to its extracellular end (Fig. 1). As expected for an ion channel (Hille 2001), Cl^- ion binding within the channel pore is thought to be an important facet of the permeation process. A recent molecular dynamics study of CFTR identified two major Cl^- ion binding sites in the pore (Zeng et al. 2023): one within the inner vestibule and including Cl^- interactions with the positively charged side-chains of K95 and R134; and one at the cytoplasmic entrance to the pore involving Cl^- interactions with K190, R248 and R303 (Fig. 1C). The functional importance of these Cl^- binding sites is demonstrated by the finding that neutralization of each of these positively charged side chains (by mutagenesis) leads to a reduction in Cl^- conductance (Ge et al. 2004; Zhou et al. 2010; El Hiani and Linsdell 2015; Li et al. 2018; Linsdell et al. 2021). Other anion binding sites may also exist (Zeng et al. 2023), including at the uncharged, narrow selectivity filter region (Linsdell 2021a).

These two major Cl^- ion binding sites are also thought to form the binding sites for anionic open-channel blockers of the pore (Linsdell 2005, 2014a; St. Aubin et al. 2007). A large

Correspondence to: Paul Linsdell, Department of Physiology and Biophysics, Dalhousie University, PO Box 15000, Halifax, Nova Scotia B3H 4R2, Canada
E-mail: paul.linsdell@dal.ca

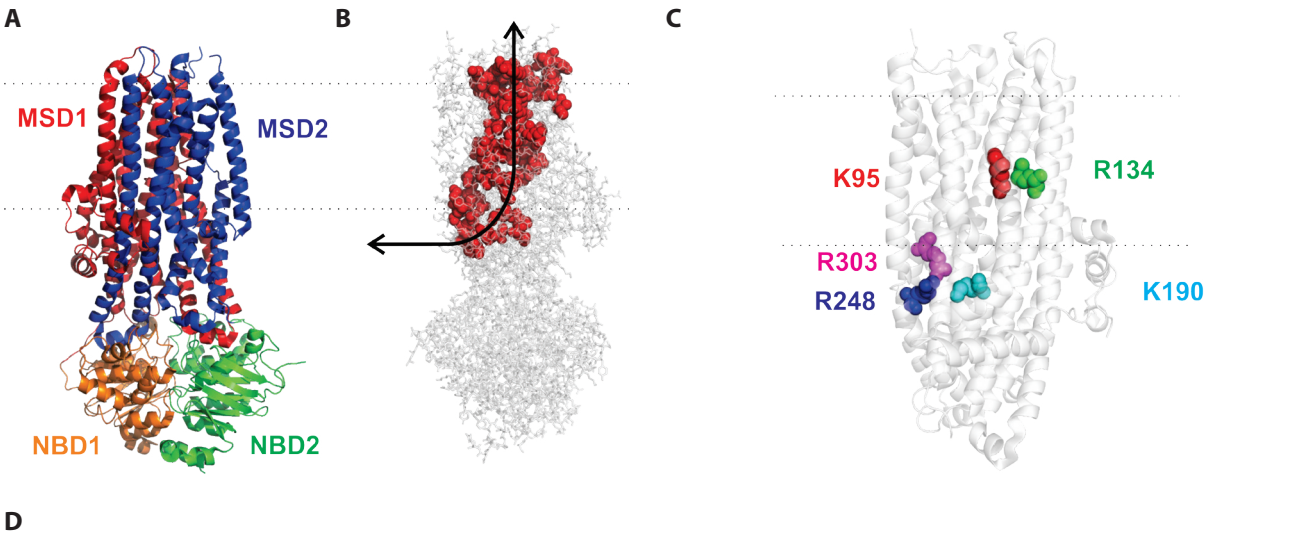

Figure 1. Structure of the CFTR pore and location of anion binding sites. **A.** Atomic structure of human CFTR in a phosphorylated, ATP-bound state (Zhang et al. 2018). Different colours represent different domains, the two membrane-spanning domains (MSD1, MSD2) and two cytoplasmic nucleotide binding domains (NBD1, NBD2). The cytoplasmic regulatory domain is absent from this structure. **B.** Location of putative pore-lining side-chains (red in space-filling models) in the same structure (Linsdell et al. 2021), and proposed pathway for Cl^- permeation (black arrow) (Linsdell 2018). **C.** Location of positively-charged side-chains proposed to contribute to anion binding sites in the inner vestibule of the pore (K95, R134) and at the cytoplasmic entrance to the pore (K190, R248, R303) (Zeng et al. 2023); same structure as (A), with NBDs removed. **D.** Spatial proximity of pore-lining side-chains mutated in the present study (E92, I344, S1141) and positively charged side-chains in the inner vestibule (K95, R134; see (C)), shown in a closer view of the same structure. In (A)–(C), dotted lines indicate the approximate extent of the membrane. (See online version for color figure.)

number of structurally diverse anions are able to penetrate from the cytoplasmic side of the membrane into the wide inner vestibule, where they bind to temporarily interrupt Cl^- permeation (Linsdell 2014a). This typically produces a voltage- and extracellular [Cl^-]-dependent block of Cl^- permeation (Linsdell 2014a; Zegarra-Moran and Galietta 2017) and is thought to involve interactions with both K95 (Linsdell 2005; Zhou et al. 2010; Linsdell 2021a) and R134 (Linsdell et al. 2021). The very large, multivalent anion suramin produces a voltage- and extracellular [Cl^-]-independent block at the cytoplasmic mouth of the pore (St. Aubin et al. 2007), involving interactions with K190, R248 and R303 (St. Aubin et al. 2007; Li et al. 2018). Open-channel blocking anions that are able to interact with these two binding sites have therefore proven highly useful probes of the structure and function of the channel pore, and of the biophysical mechanism of Cl^- permeation (Linsdell 2014a, 2021a).

The Cl^- ion binding site in the inner vestibule was described as "loosely organized" (Zeng et al. 2023), meaning that in molecular dynamics simulations Cl^- ions were usually bound to only one amino acid side-chain at a time. Consistent with this, it has been shown using mutagenesis that the important positive charges of K95 (Zhou et al. 2010; El Hiani and Linsdell 2012; Linsdell 2014b, 2015, 2021a) and R134 (Linsdell et al. 2021) can be "moved" to other nearby locations including I344 and S1141, with only minor effects on Cl^- conductance and anion binding properties (Fig. 1D). Interestingly, mutagenesis has also recently shown that a nearby *negatively* charged side-chain (E92) also contributes to anion binding in the inner vestibule, with the overall net balance between positive (K95, R134) and negative (E92) charges determining anion binding and Cl^- conductance (Linsdell et al. 2022) (Fig. 1D). Thus, whereas mutations that reduce the net "positivity" in this region (e.g. K95Q, R134Q, S1141E) drastically reduce Cl^- conductance (Ge et al. 2004; Linsdell et al. 2021, 2022) and weaken the binding of open-channel-blocking test anions (such as the high-affinity permeant anion $Au(CN)_2^-$, im-

permeant divalent anion $Pt(NO_2)_4^{2-}$, and the organic anion 5-nitro-2-(3-phenylpropylamino)benzoic acid (NPPB)) (Ge et al. 2004; Linsdell 2021a; Linsdell et al. 2021, 2022), second-site mutations that increase overall positive charge (e.g. E92Q, I344K, S1141K) restore close to wild-type-like Cl^- conductance and anion binding properties (Zhou et al. 2010; El Hiani and Linsdell 2012; Linsdell 2016; Linsdell 2021a; Linsdell et al. 2021, 2022). Interestingly, mutations that *increase* overall positivity – either by introducing an additional positive charge (e.g. I344K, S1141K) or by removing the negative charge at E92 – do not lead to a further increase in Cl^- conductance (Zhou et al. 2010; El Hiani and Linsdell 2012, 2021a; Linsdell et al. 2022), an increase in affinity of the high-affinity monovalent anion $Au(CN)_2^-$ (Linsdell 2021a; Linsdell et al. 2022), or an increase in apparent overall Cl^- binding affinity of the pore (Linsdell 2021a). Instead, the main effect of extra positive charge appears to be a drastic (up to 2–3 orders of magnitude, depending on conditions) increase in the binding affinity of divalent blocking anions such as $Pt(NO_2)_4^{2-}$ (Zhou et al. 2010; El Hiani and Linsdell 2012, 2015, 2021a) and $S_2O_3^{2-}$ (Linsdell 2021b; Linsdell et al. 2022). This has led to the suggestion that the balance of positive (K95, R134) and negative (E92) charge in the wild-type CFTR pore results in optimal binding of monovalent anions (such as Cl^-), and introducing additional positive charge in this region leads to an overall detrimental combination of no further increase in Cl^- conductance together with enhanced block of the channel by tight-binding divalent anions (Linsdell et al. 2022).

Binding of divalent $Pt(NO_2)_4^{2-}$ ions to their site in the inner vestibule of the pore also alters channel gating, slowing the opening of closed channels and possibly also slowing the closing of open channels (Linsdell 2014b). This was used to suggest that channel structural transitions involved in pore opening and closing are prevented by ion binding in the inner vestibule (Linsdell 2014b). Interestingly, mutations that strengthen open-channel block by $Pt(NO_2)_4^{2-}$ (I344K, V345K) were also shown to increase the affinity of the effect of this anion on channel gating, although the overall mechanism by which channel gating was altered appeared to be the same as for wild-type CFTR (Linsdell 2014b). However, the ability of other anions that bind within the inner vestibule to interfere with channel gating has not been reported.

Divalent anions $Pt(NO_2)_4^{2-}$ and $S_2O_3^{2-}$ have proved useful probes of the pore of both wild-type (Gong and Linsdell 2003; Zhou et al. 2007; Linsdell 2014b, 2021a, 2021b) and pore-mutant forms of CFTR (Zhou et al. 2007, 2010; El Hiani and Linsdell 2012; Linsdell 2014b, 2015, 2021a, 2021b; Linsdell et al. 2022). In contrast, trivalent anions $Co(CN)_6^{3-}$ and $Fe(CN)_6^{3-}$ were reported to have no effect on wild-type CFTR when applied to the cytoplasmic side of the channel (Gong and Linsdell 2003). More recently, trivalent $Co(NO_2)_6^{3-}$ and (to a lesser extent) $Co(CN)_6^{3-}$ and $IrCl_6^{3-}$ were shown weakly to inhibit wild-type CFTR from the extracellular solution (Li et al. 2012), suggesting some ability to interact with the pore. In an attempt to broaden the arsenal of probes available to investigate the pore, this study re-examines the effect of intracellular trivalent anions $Co(NO_2)_6^{3-}$, $Co(CN)_6^{3-}$ and $IrCl_6^{3-}$ on wild-type and pore-mutant forms of CFTR with enhanced anion binding properties.

Materials and Methods

Experiments were carried out on baby hamster kidney cells transiently transfected with human CFTR, as described previously (Zhou et al. 2010). Except where indicated (Fig. 5), experiments were carried out on very high open probability channels bearing the E1371Q mutation. As described previously, use of this E1371Q mutant allows the effects of blocking substances on Cl^- permeation through the open channel pore to be investigated in isolation from potential effects on channel gating (Zhou et al. 2010; Linsdell 2016, 2021a). Mutants used in this background (E92Q, I344K, S1141K) (Fig. 1) have been described recently (e.g. Linsdell 2021a; Linsdell et al. 2022).

Macroscopic patch clamp recordings were made from inside-out membrane patches, as described in detail previously (Zhou et al. 2010). The intracellular (bath) solution contained (mM): 150 NaCl, 2 $MgCl_2$, 10 N-tris[hydroxymethyl]methyl-2-aminoethanesulfonate (TES), pH 7.4. The extracellular (pipette) solution was the same (high [Cl^-]), or with 150 mM Na gluconate substituted for NaCl to generate an outwardly-directed [Cl^-] gradient (low [Cl^-]). Following patch excision and recording of background (leak) currents, channel activity was stimulated by exposure to protein kinase A catalytic subunit (PKA; 30 nM) plus 50 μM ATP in the intracellular solution. This relatively low concentration of ATP was used to obviate ATP block of high-affinity channels (Zhou et al. 2010) as described previously (Linsdell 2014b). Even under these low [ATP] conditions, some time-dependence of current amplitude at very negative voltages – likely reflecting ATP block (Zhou et al. 2010) – was observed for E92Q, I344K and S1141K under control conditions. Average macroscopic current amplitude was measured over a 200 ms period at the end of a 1 s duration voltage step to different test potentials from a holding potential of +88 mV (low extracellular [Cl^-]) or 0 mV (high extracellular [Cl^-]). Voltage steps were applied at a frequency of 0.29 Hz. Voltage steps – rather than ramp changes in voltage as used previously (e.g. Linsdell 2015, 2021a) – were necessary due to the pronounced time-dependence of block of mutant channel currents (Figs. 2A, 3A, 4A, 5A). Current traces were

filtered at 150 Hz, digitized at 1 kHz, and analyzed using pCLAMP10 software (Molecular Devices, Sunnyvale, CA, USA). Background (leak) currents have been subtracted digitally (Linsdell and Hanrahan 1996, 1998). Membrane voltages were corrected for liquid junction potentials calculated using pClamp software.

Block of Cl^- permeation was investigated by direct application of three different substances (sodium hexani-

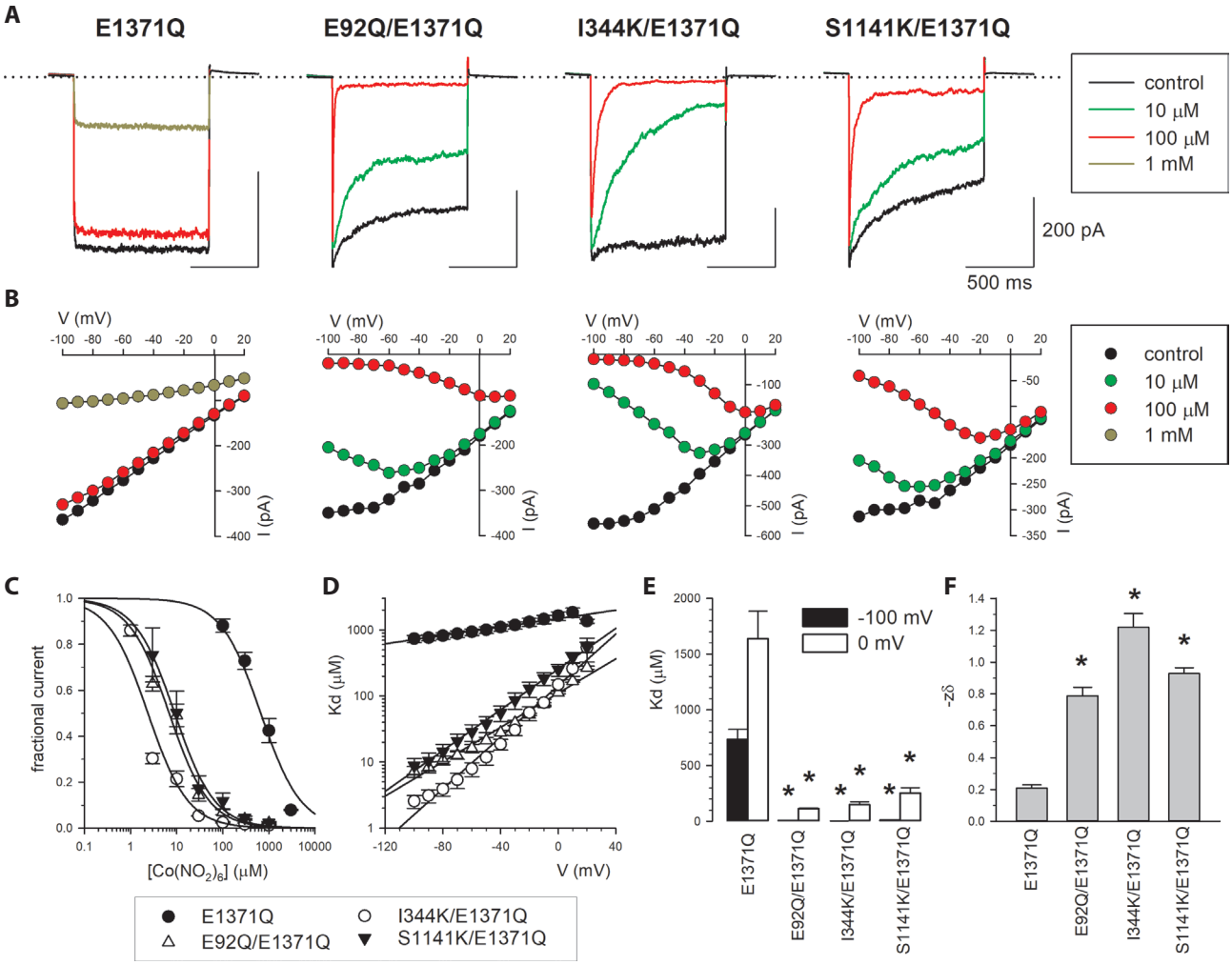

Figure 2. Inhibition of pore-mutant forms of CFTR by intracellular $Co(NO_2)_6^{3-}$ ions. **A.** Example currents from inside-out patches for the named channel variants during voltage steps (1 s duration) from a holding potential of +88 mV to a test potential of −100 mV. All channel variants studied included the E1371Q mutation to isolate effects on open channels (see Materials and Methods). Currents were recorded under low (4 mM) extracellular Cl^- conditions. Currents were recorded before (control; black lines) and following application of the named concentration of $Co(NO_2)_6^{3-}$ to the intracellular (bath) solution. Dotted line indicates zero current. **B.** Current-voltage relationships for these patches during voltage steps to different test potentials, before (control; black symbols) and following application of different concentrations of $Co(NO_2)_6^{3-}$ to the intracellular solution. **C.** Mean fractional current remaining (at −100 mV) following addition of different concentrations of $Co(NO_2)_6^{3-}$ to the intracellular solution for the named channel variants. These mean data have been fitted as described in Materials and Methods (Eq. 1) giving Kd values of 667 μM for E1371Q, 6.89 μM for E92Q/E1371Q, 2.38 μM for I344K/E1371Q and 9.07 μM for S1141K/E1371Q. Mean of data from 4 (E92Q/E1371Q, S1141K/E1371Q) or 5 (E1371Q, I344K/E1371Q) patches. **D.** Mean Kd values calculated from different patches as a function of membrane potential for the named channel variants. The slope of these graphs (logarithmic scale) was used to quantify blocker effective valence (zδ) as described in Materials and Methods (Eq. 3). **E.** Mean Kd values for different channel variants at membrane potentials of −100 mV (black bars) and 0 mV (white bars). Due to the linear scale on the *ordinate*, some black bars are very small (compare logarithmic scale in (D)). Asterisks indicate a significant difference from wild-type ($p < 0.0005$). **F.** Mean effective valence of block (−zδ) for different channel variants, calculated from individual patches as described in (D). Asterisks indicate a significant difference from wild-type ($p < 10^{-6}$). Mean of data from 6 (E92Q/E1371Q), 7 (E1371Q, S1141K/E1371Q) or 8 (I344K/E1371Q) patches in (D)–(F).

tritocobaltate (III), $Na_3Co(NO_2)_6$; sodium cobalticyanide, $Na_3Co(CN)_6$; sodium hexachloroiridate (III), Na_3Ir_6) to the intracellular face of inside-out patches. These substances were initially solubilized as high-concentration (100 mM) aqueous stock solutions, then diluted to the final concentrations using normal bath solution. Blocker

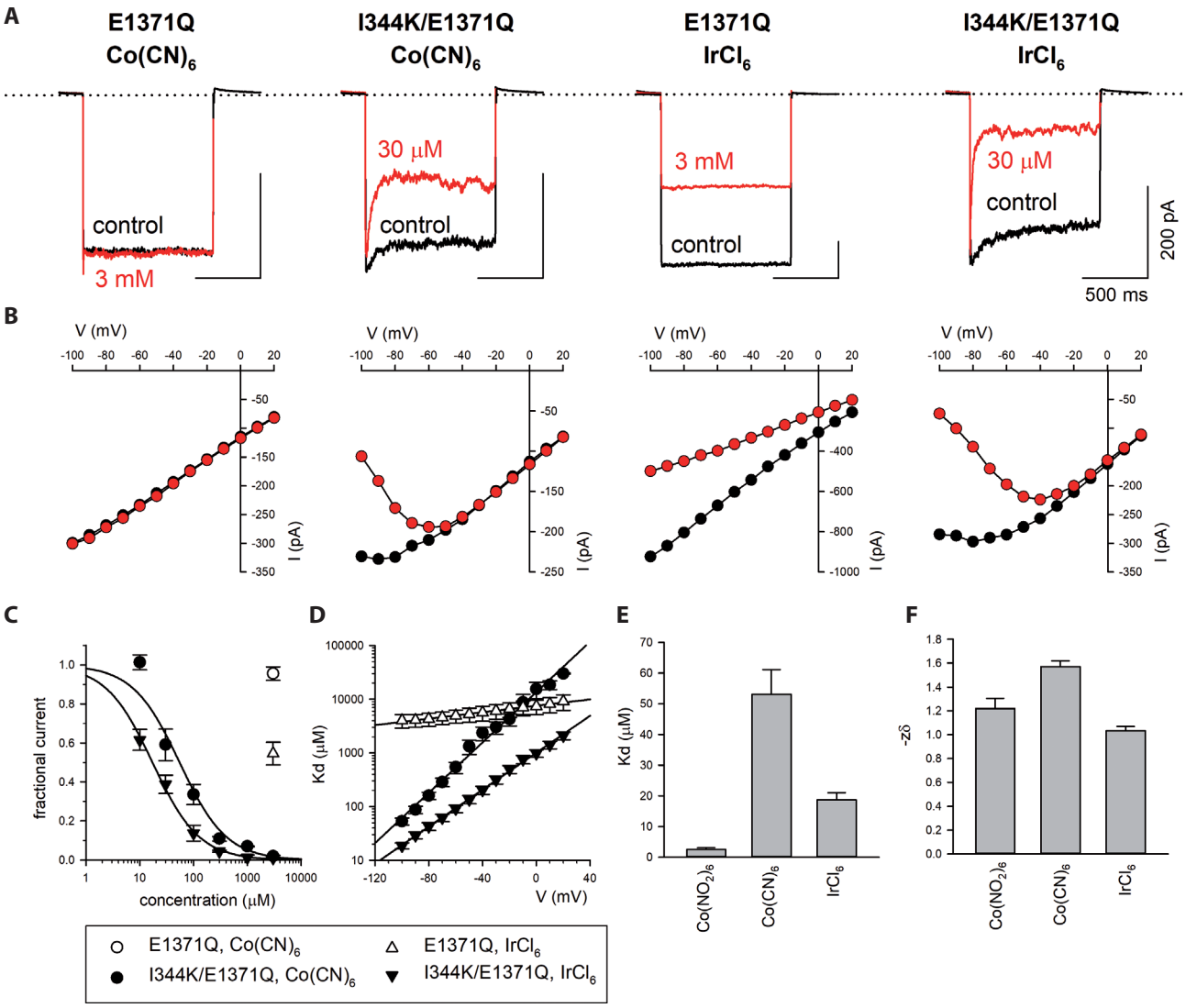

Figure 3. Inhibition of E1371Q and I344K/E1371Q by intracellular $Co(CN)_6^{3-}$ and $IrCl_6^{3-}$ ions. A. Example currents from inside-out patches for E1371Q and I344K/E1371Q under the same conditions used in Figure 2. Currents were recorded before (control; black lines) and following application of the named concentration of $Co(CN)_6^{3-}$ or $IrCl_6^{3-}$ the intracellular (bath) solution as indicated (red lines). Dotted line indicates zero current. **B.** Current-voltage relationships for these patches during voltage steps to different test potentials, before (control; black symbols) and following application of these concentrations of $Co(CN)_6^{3-}$ or $IrCl_6^{3-}$ to the intracellular solution (red symbols). **C.** Mean fractional current remaining (at −100 mV) following addition of different concentrations of $Co(CN)_6^{3-}$ or $IrCl_6^{3-}$ to the intracellular solution for I344K/E1371Q (black symbols); due to weak inhibition of E1371Q, only the effects of 3 mM $Co(CN)_6^{3-}$ or $IrCl_6^{3-}$ were quantified (white symbols). For I344K/E1371Q, mean data have been fitted as described in Materials and Methods (Eq. 1), giving Kd values of 54.9 μM for $Co(CN)_6^{3-}$ and 17.2 μM for $IrCl_6^{3-}$. Mean of data from 4 (E1371Q) or 5 (I344K/E1371Q) patches. **D.** Mean Kd values calculated from different patches as a function of membrane potential for E1371Q (white symbols; calculated as described in Materials and Methods (Eq. 2)) and I344K/E1371Q (black symbols). The slope of these graphs was used to quantify blocker effective valence (zδ) as in Figure 2. **E.** Comparison of mean Kd values (at −100 mV) for different blocking anions for I344K/E1371Q channels. **F.** Comparison of mean −zδ values for these same blocking anions in I344K/E1371Q channels. Mean of data from 9 patches in (D)–(F), except 4 patches for E1371Q in (D), and 8 patches for I344K ($Co(NO_2)_6^{3-}$) in (E) and (F). (See online version for color figure.)

concentration-inhibition relationships were fitted by the equation:

$$\text{Fractional unblocked current} = \frac{1}{1 + ([B]/Kd)} \quad (1)$$

where [B] is blocker concentration, and Kd is the apparent blocker dissociation constant. Low-affinity block of wild-type by $IrCl_6^{3-}$ (Fig. 3) was quantified using the effects of a single, high concentration of this blocker, according to the equation:

$$Kd = \frac{[B]}{[1/(I/I0)] - 1} \quad (2)$$

where I is current amplitude following the addition of blocker, and I_0 is the control, unblocked current amplitude. The relationship between Kd and applied membrane potential (V) was fitted by the equation:

$$Kd(V) = \text{Kd}(0)\ e^{-z\delta VF/RT} \quad (3)$$

where zδ is the measured effective valence of the blocking ion (actual valence (z) multiplied by the fraction of the transmembrane electric field apparently experienced during the blocking reaction (δ)), and F, R and T have their usual thermodynamic meanings.

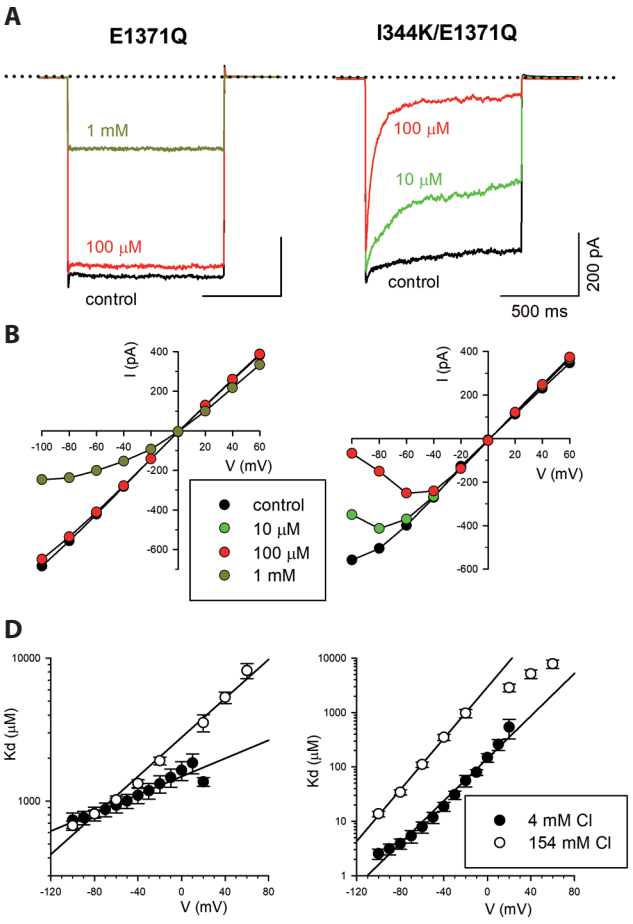

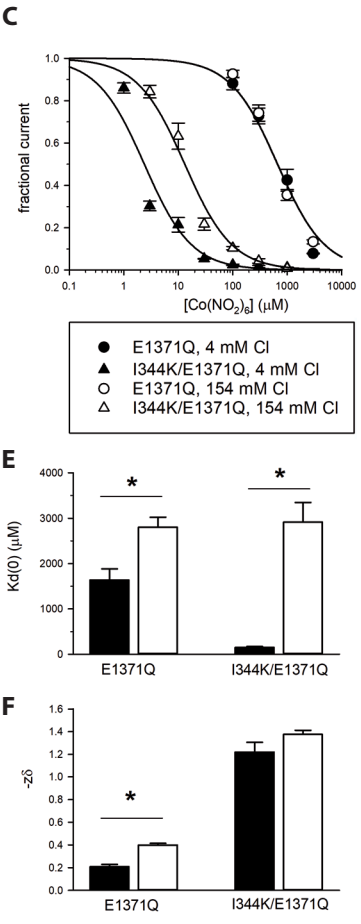

Figure 4. Inhibition of E1371Q and I344K/E1371Q by intracellular $Co(NO_2)_6^{3-}$ under high extracellular [Cl^-] conditions. **A.** Example currents from inside-out patches for E1371Q (left) and I344K/E1371Q (right) during voltage steps (1 s duration) from a holding potential of 0 mV to a test potential of −100 mV. Currents were recorded under high (154 mM) extracellular Cl^- conditions. Currents were recorded before (control; black lines) and following application of the named concentration of $Co(NO_2)_6^{3-}$ to the intracellular (bath) solution (same colour scheme as in Fig. 2). Dotted line indicates zero current. **B.** Current-voltage relationships for these patches during voltage steps to different test potentials, before (control; black symbols) and following application of different concentrations of $Co(NO_2)_6^{3-}$ to the intracellular solution. **C.** Mean fractional current remaining (at −100 mV) following addition of different concentrations of $Co(NO_2)_6^{3-}$ to the intracellular solution for E1371Q (circles) and I334K/E1371Q (triangles), under low (4 mM; black symbols) and high (154 mM; white symbols) extracellular Cl^- conditions. These mean data have been fitted as described in Materials and Methods (Eq. 1) giving Kd values of 667 µM for E1371Q and 2.38 µM for I344K/E1371Q (4 mM Cl^-; see Fig. 2), and 663 µM for E1371Q and 13.2 µM for I344K/E1371Q (154 mM Cl^-). Mean of data from 5 patches, except 4 patches for E1371Q (154 mM Cl^-). **D.** Mean Kd values calculated from different patches as a function of membrane potential for E1371Q (left panel) and I344K/E1371Q (right panel). The slope of these graphs was used to quantify blocker effective valence (zδ) as in Figure 2. Note the different scale to the *ordinate* in these two panels; voltage-dependence of block was much stronger in I344K, as quantified in (F). **E.** Mean Kd values at a membrane potentials of 0 mV under low (black bars) and high [Cl^-] conditions (white bars). *Asterisks* indicate a significant difference depending on [Cl^-] ($p < 0.005$). **F.** Mean effective valence of block (−zδ) under low (black bars) and high [Cl^-] conditions (white bars). *Asterisk* indicates a significant difference depending on [Cl^-] ($p < 10^{-5}$). Mean of data from 7 (E1371Q (4 mM Cl^-), 8 (E1371Q (154 mM Cl^-); I344K/E1371Q (4 mM Cl^-)) or 9 (I344K/E1371Q (154 mM Cl^-) patches in (D)–(F).

Experiments were carried out at room temperature, 21–24°C. Values are presented as mean ± SEM. For graphical presentation of mean values, error bars represent SEM, and where no error bars are visible SEM is smaller than the size of the symbol. Tests of significance were carried out using Student's two-tailed *t*-test, with $p < 0.05$ being considered statistically significant. All chemicals were from Sigma-Aldrich (Oakville, ON, Canada), except for PKA (Promega, Madison, WI, USA), $Na_3Co(NO_2)_6$ and $Na_3Co(CN)_6$ (Strem Chemicals, Newburyport, MA, USA), and Na_3IrCl_6 (City Chemical LLC, West Haven, CT, USA).

Results

Open-channel block by trivalent ions is strengthened by pore mutations

Block by intracellular $Co(NO_2)_6^{3-}$ ions was investigated by application to the intracellular face of inside-out patches, under low (4 mM) extracellular [Cl^-] conditions. In order to isolate effects on open channels, these experiments were carried out on channels bearing the E1371Q mutation (see Materials and Methods). Relatively high concentrations (> 100 μM) of $Co(NO_2)_6^{3-}$ caused a time-independent, weakly voltage-dependent inhibition of E1371Q channel currents (Fig. 2). Introduction of a number of pore mutations that have previously been associated with strong anion binding (E92Q, I344K, S1141K) resulted in a dramatic increase in both the affinity of block by $Co(NO_2)_6^{3-}$ and in the voltage-dependence of block (Fig. 2). Furthermore, block of each of these pore-mutants channels was strongly time-dependent at negative voltages (Fig. 2A), necessitating the use of voltage steps rather than ramp changes in voltage as used previously (e.g. Linsdell 2015, 2021). Analysis of the concentration- and voltage-dependence of inhibition (Fig. 2C,D) revealed that these three pore mutations increased the apparent affinity of block by 80–280-fold (at −100 mV) and 6–14-fold (at 0 mV) (Fig. 2E), and dramatically increased the apparent voltage-dependence of block (quantified as effective valence of block, zδ; Fig. 2F).

Since I344K/E1371Q was the mostly strongly blocked by $Co(NO_2)_6^{3-}$ ions, block of this mutant by other trivalent anions was also investigated. As shown in Figure 3, both $Co(CN)_6^{3-}$ and $IrCl_6^{3-}$ ions also caused a strong, time- and voltage-dependent block of I344K/E1371Q channels. In contrast, $IrCl_6^{3-}$ caused only weak, time-independent block of E1371Q, and $Co(CN)_6^{3-}$ had no apparent effect at concentrations as high as 3 mM (Fig. 3). Comparison of the effects of these three trivalent anions on high-affinity I344K/E1371Q channels (Fig. 3E,F) revealed that $Co(NO_2)_6^{3-}$ was the most effective blocker, with an apparent affinity (at −100 mV) >7-fold higher than $IrCl_6^{3-}$ ($p < 0.00005$) and >20-fold higher than $Co(CN)_6^{3-}$ ($p < 0.00005$). All three blockers had similarly strong voltage-dependence in this mutant (Fig. 3F).

Effect of extracellular Cl^- on block by $Co(NO_2)_6^{3-}$

In order to investigate interactions between intracellular $Co(NO_2)_6^{3-}$ and extracellular Cl^- – as well as to allow investigation of block at more positive voltages to facilitate the investigation of the relationship between block and gating (see below) – block by $Co(NO_2)_6^{3-}$ was also studied under high (154 mM) extracellular [Cl^-] conditions. Under these conditions, block of E1371Q was slightly weakened (~1.7-fold increase in Kd at 0 mV) (Fig. 4C–E) and significantly more strongly voltage-dependent (Fig. 4D, F). Block of I344K/E1371Q was more drastically weakened at high extracellular [Cl^-] (>19-fold increase in Kd at 0 mV) (Fig. 4C-E), however, voltage-dependence of block (at negative voltages where block was stronger and could be more reliably quantified) was not significantly changed ($p > 0.1$) (Fig. 4D,F).

Relationship between $Co(NO_2)_6^{3-}$ block and gating in I344K-mutant channels

High-affinity binding of divalent $Pt(NO_2)_4^{2-}$ ions strongly affects the gating of high-affinity mutant channels including I344K (Linsdell 2014b), an effect that is readily apparent by comparing the blocking effects on open (E1371Q-containing) channels with those on channels that are opening and closing normally (wild-type background) (Linsdell 2014b). However, in contrast to the strong difference in the affinity and voltage-dependence of $Pt(NO_2)_4^{2-}$ block observed in these two backgrounds (Linsdell 2014b), block by $Co(NO_2)_6^{3-}$ was essentially unchanged between I344K channels (wild-type background) and I344K/E1371Q (Fig. 5).

Discussion

Probes of anion binding sites in the CFTR pore

Anion binding sites in CFTR have been probed using a number of anions that bind with sufficiently high affinity to block Cl permeation, including relatively large organic anions (Linsdell 2014a), smaller, highly lyotropic monovalent anions such as SCN^- (Mansoura et al. 1998; Linsdell 2001) and $Au(CN)_2^-$ (Smith et al. 1999; Gong et al. 2002; Linsdell 2021a), as well as divalent anions such as $Pt(NO_2)_4^{2-}$ (Gong and Linsdell 2003; Zhou et al. 2007; Linsdell 2021a) and $S_2O_3^{2-}$ (Linsdell 2021b; Linsdell et al. 2023). Compared to some of these probes, the trivalent anions used in the present study have relatively weak blocking effects on the

wild-type CFTR pore. Using E1371Q-containing channels to isolate effects on open channels, the most effective anion used, $Co(NO_2)_6^{3-}$, had a Kd of 734 ± 90 μM (n = 7) under the most optimal conditions studied (−100 mV, low extracellular [Cl^-]) (Fig. 2C–E). Under similar conditions, the Kd for $IrCl_6^{3-}$ was 4.04 ± 1.14 mM (n = 4) (Fig. 3D), while $Co(CN)_6^{3-}$ had no apparent blocking effect at concentrations as high as 3 mM (Fig. 3 A–C). For comparison, under the same experimental conditions, this lab has recently reported Kd values of ~54 μM for monovalent $Au(CN)_2^-$ ions, and ~40 μM for divalent $Pt(NO_2)_4^{2-}$ ions (Linsdell 2021a). As with most intracellular blocking anions, block was weakened both by depolarizing voltages (Fig. 2D–F; Fig. 3D) and (for $Co(NO_2)_6^{3-}$ at least) by extracellular Cl^- (Fig. 4D–F). Thus it appears that small multivalent anions are not useful as high-affinity probes of the wild-type pore. One possibility is that the high charge density of these anions disfavours anion dehydration inside the pore, preventing these anions from approaching closely to anion binding sites. Alternatively, these same physical properties may impede trivalent anion entry into the pore from the cytoplasmic solution.

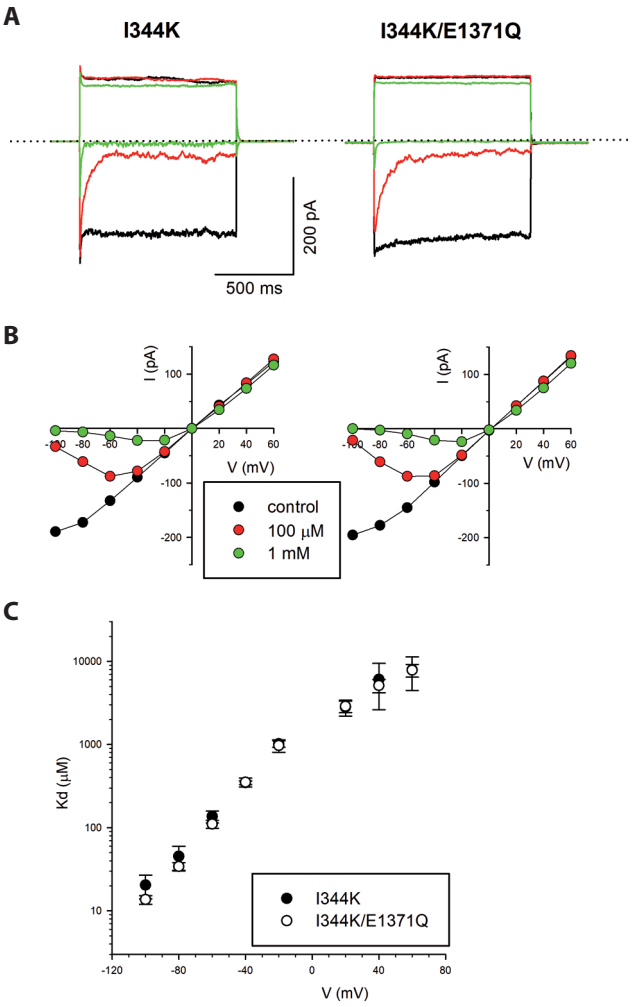

Figure 5. Effect of E1371Q mutation on high-affinity block of I344K by $Co(NO_2)_6^{3-}$. **A.** Example currents from inside-out patches for I344K E1371Q and I344K/E1371Q during voltage steps (1 s duration) from a holding potential of 0 mV to a test potentials of +60 mV (positive currents) and −100 mV (negative currents). Currents were recorded under high (154 mM) extracellular Cl^- conditions (see Fig. 4). Currents were recorded before (control; black lines) and following application of the named concentrations of $Co(NO_2)_6^{3-}$ to the intracellular (bath) solution. **B.** Current-voltage relationships for these patches during voltage steps to different test potentials, before (control; black symbols) and following application of different concentrations of $Co(NO_2)_6^{3-}$ to the intracellular solution. **C.** Mean Kd values calculated from different patches as a function of membrane potential for I344K (black symbols) and I344K/E1371Q (white symbols). The slope of these graphs was used to quantify blocker effective valence (zδ) as in Figures 2 and 4. Mean of data from 6 (I344K) or 9 (I344K/E1371Q) patches.

Block by each of these trivalent anions is drastically strengthened by mutations that alter the charge balance in the inner vestibule of the pore. For the most effective anion used, $Co(NO_2)_6^{3-}$, three different mutations (E92Q, I344K, S1141K) had very similar effects. Using E1371Q-containing channels to isolate effects on open channels, each of these mutations caused: (i) a decrease in Kd of 80–280-fold (at −100 mV; Fig. 2E), indicating strong binding affinity in the pore; (ii) a large increase in the voltage-dependence of block (3.8–5.9-fold increase in zδ; Fig. 2F); and (iii) the appearance of a strong time-dependence of block (Fig. 2A), necessitating the use of step changes in membrane potential. For I344K/E1371Q channels at least, the affinity of $Co(NO_2)_6^{3-}$ block also showed a greatly increased dependence on extracellular [Cl^-] (Fig. 4C–E), although the voltage-dependence of block of I344K/E1371Q was not sensitive to extracellular [Cl^-] (Fig. 4D,F). Overall the effects of these mutations (E92Q, I344K, S1141K) on the affinity, voltage-dependence, and Cl^--dependence of block are very similar to the effects of these same mutations on block by divalent $Pt(NO_2)_4^{2-}$ ions (Zhou et al. 2010; El Hiani and Linsdell 2012, 2021a). I344K also showed similar striking increases in the affinity, voltage-dependence, and time-dependence of block by two other trivalent anions, $Co(CN)_6^{3-}$ and $IrCl_6^{3-}$ (Fig. 3), although these two anions were less potent blockers of this mutant channel than was $Co(NO_2)_6^{3-}$ (Fig. 3E). Together this suggests that the trivalent anions $Co(NO_2)_6^{3-}$, $Co(CN)_6^{3-}$ and $IrCl_6^{3-}$ show similar interactions with high-affinity binding-site mutants (e.g. E92Q, I344K, S1141K) as previously shown for the high-affinity probe $Pt(NO_2)_4^{2-}$ (Zhou et al. 2010; El Hiani and Linsdell 2012; Linsdell 2021a). Detailed analysis of $Pt(NO_2)_4^{2-}$ block of I344K/E1371Q suggested that the increased voltage-dependence and increased extracellular [Cl^-]-dependence of block resulted primarily from strengthened interactions between $Pt(NO_2)_4^{2-}$ and

Cl^- ions inside the pore, as well as changes in the affinity and voltage-dependence of Cl^- binding to the pore (Linsdell 2015). Similar effects likely underlie the increased voltage- and [Cl^-]-dependence of block observed for trivalent anion blockers. However, these blockers show much lower affinity than $Pt(NO_2)_4^{2-}$. For example, the most potent of these trivalent anions, $Co(NO_2)_6^{3-}$, inhibits I344K/E1371Q channels with a Kd of 149 ± 27 μM (n = 6) at 0 mV (Fig. 2D,E), compared to ~7 μM for $Pt(NO_2)_4^{2-}$ recently reported by this lab under similar experimental conditions (Linsdell 2021a). Thus, even when anion binding affinity is increased by mutagenesis, the pore still appears to disfavour binding of trivalent anions. It is tempting to speculate that the same mechanism(s) that prevents high affinity binding of these anions to the wild-type pore (see above) is still present in these mutant channel pores.

Mutations that alter the charge balance in the inner vestibule, either by introducing additional positive charge (e.g. I334K, S1141K) or by removing endogenous negative charge (e.g. E92Q) have previously been shown to greatly increase the affinity and voltage-dependence of block by small divalent anions $Pt(NO_2)_4^{2-}$ (Zhou et al. 2010; El Hiani and Linsdell 2012; Linsdell 2021a) and $S_2O_3^{2-}$ and SO_4^{2-} (Linsdell 2021b; Linsdell et al. 2022). In contrast, these mutations have little effect on block by monovalent $Au(CN)_2^-$ ions (Linsdell 2021a; Linsdell et al. 2022), even though $Au(CN)_2^-$ and $Pt(NO_2)_4^{2-}$ appear to share a common molecular mechanism of block of wild-type CFTR (Ge et al. 2004; Zhou et al. 2007; Linsdell 2021a). These mutations have also been suggested to have little impact on the binding affinity of Cl^- ions themselves within the pore (Linsdell 2021a). This has led to the suggestion that altering the charge balance within the inner vestibule of the pore favours the binding of divalent over monovalent anions (Zhou et al. 2010; Linsdell 2021a, 2021b), perhaps indicating that the wild-type pore is well optimized for monovalent anion binding and permeation (Linsdell 2021b). Perhaps unsurprisingly, the current results with trivalent anions $Co(NO_2)_6^{3-}$, $Co(CN)_6^{3-}$ and $IrCl_6^{3-}$ suggest that this model should be extended to state that charge-altering mutations favour the binding of multivalent over monovalent anions.

The relationship between anion binding and channel gating

The preceding discussion relates to the effects of blocking anions on open channels. An interesting facet of $Pt(NO_2)_4^{2-}$ block of high-affinity channels such as I344K is that the high affinity of block also facilitates the detection of blocker effects on channel gating (an effect that is also observed – albeit at much lower affinity – in wild-type channels) (Linsdell 2014b). This effect – in which $Pt(NO_2)_4^{2-}$ binding appears to slow both the opening and closing of the channel – is most readily identified as a dramatic change in the affinity and voltage-dependence of block of macroscopic currents when comparing E1371Q and wild-type (1371E) channel backgrounds (Linsdell 2014b). Thus a major difference between the effects of $Co(NO_2)_4^{3-}$ reported here and those of $Pt(NO_2)_4^{2-}$ reported previously is the apparently identical effects of $Co(NO_2)_4^{3-}$ on I344K and I344K/E1371Q channels (Fig. 5). This suggests that high-affinity $Co(NO_2)_4^{3-}$ block of this mutant has no impact on the opening and closing of the channel. The differences between $Pt(NO_2)_4^{2-}$ and $Co(NO_2)_4^{3-}$ – and their interactions with the pore – that mean that $Pt(NO_2)_4^{2-}$ binding in the inner vestibule appears to slow or prevent both opening and closing (Linsdell 2014b), whereas $Co(NO_2)_4^{3-}$ binding presumably does not (Fig. 5) – are not currently known. Nevertheless, these differences do offer some encouragement that these anions can be used differentially to probe the interaction between anion binding in the pore and channel gating.

Conclusions

The small trivalent anions $Co(NO_2)_6^{3-}$, $Co(CN)_6^{3-}$ and $IrCl_6^{3-}$ are not particularly high-affinity probes of the wild-type CFTR pore, consistent with CFTR showing strong preference for monovalent anions (Linsdell 2021b). Where anion binding within the pore is artificially strengthened by mutagenesis, both the affinity and voltage-dependence of block by these substances is greatly enhanced, as reported previously for the divalent anion probes $Pt(NO_2)_4^{2-}$ (Zhou et al. 2010; El Hiani and Linsdell 2012; Linsdell 2021a) and $S_2O_3^{2-}$ (Linsdell 2021b; Linsdell et al. 2022). However, these trivalent probes still appear to bind with much lower affinity than $Pt(NO_2)_4^{2-}$, suggesting that some charge valence selectivity still exists in these mutants. These anions increase the arsenal of probes that can be used to investigate the structure and function of Cl^- channel pores, as well as potentially the relationship between anion binding and the distribution of fixed charges within channel pores, and the relationship between anion binding and channel gating.

Conflicts of interest. The author has no conflict of interest to declare.

Acknowledgements. I would like to thank Christina Irving for technical assistance. This work was supported by a grant from the Natural Sciences and Engineering Research Council of Canada (RGPIN/05124-2017).

References

Csanády L, Vergani P, Gadsby DC (2019): Structure, gating, and regulation of the CFTR anion channel. Physiol. Rev. **99,** 707-738 https://doi.org/10.1152/physrev.00007.2018

El Hiani Y, Linsdell P (2012): Tuning of CFTR chloride channel function by location of positive charges within the pore. Biophys. J. **103,** 1719-1726
https://doi.org/10.1016/j.bpj.2012.09.020

El Hiani Y, Linsdell P (2015): Functional architecture of the cytoplasmic entrance to the cystic fibrosis transmembrane conductance regulator chloride channel pore. J. Biol. Chem. **290,** 15855-15865
https://doi.org/10.1074/jbc.M115.656181

Farkas B, Tordai H, Padányi R, Tordai A, Gera J, Paragi G, Hegedüs T (2020): Discovering the chloride pathway in the CFTR channel. Cell. Mol. Life Sci. **77,** 765-778
https://doi.org/10.1007/s00018-019-03211-4

Ge N, Muise CN, Gong X, Linsdell P (2004): Direct comparison of the functional roles played by different membrane spanning regions in the cystic fibrosis transmembrane conductance regulator chloride channel pore. J. Biol. Chem. **279,** 55283-55289
https://doi.org/10.1074/jbc.M411935200

Gong X, Burbridge SM, Cowley EA, Linsdell P (2002): Molecular determinants of Au(CN)¬2- binding and permeability within the cystic fibrosis transmembrane conductance regulator Cl- channel pore. J. Physiol. **540,** 39-47
https://doi.org/10.1113/jphysiol.2001.013235

Gong X, Linsdell P (2003): Mutation-induced blocker permeability and multiion block of the CFTR chloride channel pore. J. Gen. Physiol. **122,** 673-687
https://doi.org/10.1085/jgp.200308889

Hille B (2001): Ion Channels of Excitable Membranes (3rd Ed.), Sinauer Associates

Hoffmann B, Elbahnsi A, Lehn P, Décout J-L, Pietrucci F, Mornon J-P, Callebaut I (2018): Combining theoretical and experimental data to decipher CFTR 3D structures and functions. Cell. Mol. Life Sci. **75,** 3829-3855
https://doi.org/10.1007/s00018-018-2835-7

Hwang T-C, Yeh J-T, Zhang J, Yu Y-C, Yeh H-I, Destefano S (2018): Structural mechanisms of CFTR function and dysfunction. J. Gen. Physiol. **150,** 539-570
https://doi.org/10.1085/jgp.201711946

Li M-S, Cowley EA, Linsdell P (2012): Pseudohalide anions reveal a novel extracellular site for potentiators to increase CFTR function. Br. J. Pharmacol. **167,** 1062-1075
https://doi.org/10.1111/j.1476-5381.2012.02041.x

Li, M-S, Cowley EA, El Hiani Y, Linsdell P (2018): Functional organization of cytoplasmic portals controlling access to the cystic fibrosis transmembrane conductance regulator (CFTR) chloride channel pore. J. Biol. Chem. **293,** 5649-5658
https://doi.org/10.1074/jbc.RA117.001373

Linsdell P (2001): Thiocyanate as a probe of the cystic fibrosis transmembrane conductance regulator chloride channel pore. Can. J. Physiol. Pharmacol. **79,** 573-579
https://doi.org/10.1139/y01-041

Linsdell P (2005): Location of a common inhibitor binding site in the cytoplasmic vestibule of the cystic fibrosis transmembrane conductance regulator chloride channel pore. J. Biol. Chem. **280,** 8945-8950
https://doi.org/10.1074/jbc.M414354200

Linsdell P (2014a): Cystic fibrosis transmembrane conductance regulator chloride channel blockers: pharmacological, biophysical and physiological relevance. World J. Biol. Chem. **5,** 26-39
https://doi.org/10.4331/wjbc.v5.i1.26

Linsdell P (2014b): State-dependent blocker interactions with the CFTR chloride channel: implications for gating the pore. Pflügers Arch. **466,** 2243-2255
https://doi.org/10.1007/s00424-014-1501-7

Linsdell P (2015): Interactions between permeant and blocking anions inside the CFTR chloride channel pore. Biochim. Biophys. Acta **1848,** 1573-1590
https://doi.org/10.1016/j.bbamem.2015.04.004

Linsdell P (2016): Anion conductance selectivity mechanism of the CFTR chloride channel. Biochim. Biophys. Acta **1858,** 740-747
https://doi.org/10.1016/j.bbamem.2016.01.009

Linsdell P (2017): Architecture and functional properties of the CFTR channel pore. Cell. Mol. Life Sci. **74,** 67-83
https://doi.org/10.1007/s00018-016-2389-5

Linsdell P (2018): Cystic fibrosis transmembrane conductance regulator (CFTR): Making an ion channel out of an active transporter structure. Channels **12,** 284-290
https://doi.org/10.1080/19336950.2018.1502585

Linsdell P (2021a): On the relationship between anion binding and chloride conductance in the CFTR anion channel. Biochim. Biophys. Acta **1863,** 183558
https://doi.org/10.1016/j.bbamem.2021.183558

Linsdell P (2021b): Monovalent: divalent anion selectivity in the CFTR channel pore. Cell Biochem. Biophys. **79,** 863-871
https://doi.org/10.1007/s12013-021-00998-7

Linsdell P, Hanrahan JW (1996): Disulphonic stilbene block of cystic fibrosis transmembrane conductance regulator Cl- channels expressed in a mammalian cell line and its regulation by a critical pore residue. J. Physiol. **496,** 687-693
https://doi.org/10.1113/jphysiol.1996.sp021719

Linsdell P, Hanrahan JW (1998): Adenosine triphosphate-dependent asymmetry of anion permeation in the cystic fibrosis transmembrane conductance regulator chloride channel. J. Gen. Physiol. **111,** 601-614
https://doi.org/10.1085/jgp.111.4.601

Linsdell P, Irving CL, Cowley EA (2022): Functionally additive fixed positive and negative charges in the CFTR channel pore control anion binding and conductance. J. Biol. Chem. **298,** 101659
https://doi.org/10.1016/j.jbc.2022.101659

Linsdell P, Irving CL, Cowley EA, El Hiani Y (2021): Two positively charged amino acid side-chains in the inner vestibule of the CFTR channel pore play analogous roles in controlling anion binding and anion conductance. Cell. Mol. Life Sci. **78,** 5213-5223
https://doi.org/10.1007/s00018-021-03859-x

Mansoura MK, Smith SS, Choi AD, Richards NW, Strong TV, Drumm ML, Collins FS, Dawson DC (1998): Cystic fibrosis transmembrane conductance regulator (CFTR) anion binding as a probe of the pore. Biophys. J. **74,** 1320-1332
https://doi.org/10.1016/S0006-3495(98)77845-2

Ong T, Ramsey BW (2023): Cystic fibrosis: a review. JAMA **329,** 1859-1871
https://doi.org/10.1001/jama.2023.8120

St. Aubin CN, Zhou J-J, Linsdell P (2007): Identification of a second blocker binding site at the cytoplasmic mouth of the cystic fibrosis transmembrane conductance regulator chloride channel pore. Mol. Pharmacol. **71,** 1360-1368 https://doi.org/10.1124/mol.106.031732

Smith SS, Steinle ED, Meyerhoff ME, Dawson DC (1999): Cystic fibrosis transmembrane conductance regulator: physical basis for lyotropic anion selectivity patterns. J. Gen. Physiol. **114,** 799-817 https://doi.org/10.1085/jgp.114.6.799

Zegarra-Moran O, Galietta LJV (2017): CFTR pharmacology. Cell. Mol. Life Sci. **74,** 117-128 https://doi.org/10.1007/s00018-016-2392-x

Zeng ZW, Linsdell P, Pomès R (2023): Molecular dynamics study of Cl- permeation through cystic fibrosis transmembrane conductance regulator (CFTR). Cell. Mol. Life Sci. **80,** 51 https://doi.org/10.1007/s00018-022-04621-7

Zhang Z, Liu F, Chen J (2018): Molecular structure of the ATP-bound, phosphorylated human CFTR. Proc. Natl. Acad. Sci. USA **115,** 12757-12762 https://doi.org/10.1073/pnas.1815287115

Zhou J-J, Fatehi M, Linsdell P (2007): Direct and indirect effects of mutations at the outer mouth of the CFTR chloride channel pore. J. Membr. Biol. **216,** 129-142 https://doi.org/10.1007/s00232-007-9056-6

Zhou J-J, Li M-S, Qi J, Linsdell P (2010): Regulation of conductance by the number of fixed positive charges in the intracellular vestibule of the CFTR chloride channel pore. J. Gen. Physiol. **135,** 229-245 https://doi.org/10.1085/jgp.200910327

Received: September 18, 2023
Final version accepted: December 6, 2023